Journal of Physics: Conference Series **3224** (2026) 032077 doi:10.1088/1742-6596/3224/3/032077

The impact of the turbine model on gravity wave simulations

T Rafferty[1] **and C.R Vogel**[1]

[1]Department of Engineering Science, University of Oxford, Oxford, OX1 3PJ, United Kingdom

E-mail: timothy.rafferty@eng.ox.ac.uk

Abstract. With the continued growth of wind farm capacity, it is increasingly important for wind farm developers to be able to accurately predict the interactions between wind turbines and large-scale atmospheric phenomena such as gravity waves. Simulating scenarios containing gravity waves requires multi-stage simulations in domains spanning tens of kilometres. To reduce computational costs, lower order actuator models are therefore often used to represent turbines. In this work, Large Eddy Simulations (LES) were performed using an Actuator Disk (AD) model and the higher fidelity Actuator Line (AL) model to assess how turbine representation impacts the predicted atmospheric gravity wave field and turbine wake. Furthermore, the sensitivity of the AD model predictions to mesh resolution and the model's thrust coefficient were evaluated. The results showed that the gravity wave field produced was largely independent of the chosen actuator model. However, the predicted wake shape, length, and velocity profile varied considerably between the actuator models and with the level of mesh resolution at the AD rotor plane. Overall, the turbine thrust magnitude was found to have the greatest influence on the predicted gravity waves. Since turbine wake characteristics were also shown to be heavily impacted by the wave field that develops, correct thrust prediction was therefore found to be important for farm-scale performance predictions that account for atmospheric gravity waves.

1. Introduction

With the growth of wind turbine size and the number of turbines in a wind farm, farm-scale atmospheric interactions have been observed in simulations [1]. Of particular interest is the potential for turbines to trigger Atmospheric Gravity Waves (AGWs), a phenomenon formerly only usually considered in the meteorology of mountains [2]. Multiple studies have now shown that for sufficiently large wind farms, AGWs can be triggered [3–7]. This is especially possible for wind farms in the North Sea where the inversion layer of the Conventionally Neutral Boundary Layer (CNBL) is often close to the vertical extent of large turbines (see Figure 1) [8]. Vertical displacement of the thermally stratified flow triggers buoyancy-driven waves in both the geostrophic and inversion layers. The AGWs subsequently cause a redistribution of energy, impacting power production and its distribution through a farm [9].

To accurately resolve AGWs, large domains of tens of kilometres including damping regions are required [10]. Consequently, lower-fidelity farm models are often used to achieve computational feasibility. Actuator Disk (AD) models are used most often where turbines are individually represented in such studies, with the influence of the rotor distributed over its swept area. Higher-fidelity Actuator Line (AL) models are available when greater detail around unsteady blade loads and wake dynamics are desired, albeit at the expense of higher

computational cost. Additionally, unlike the AD model, the AL simulation can capture coherent structures such as blade tip and root vortices, which can influence the wake dynamics.

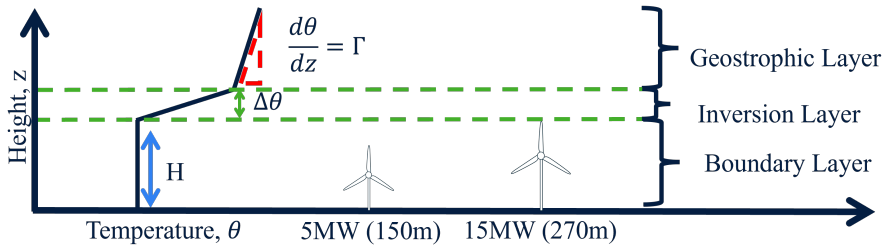

Figure 1: The Conventionally-Neutral Boundary Layer (CNBL) temperature profile compared to typical offshore wind turbine sizes. H is the temperature profile inversion height, $\Delta\theta$ the strength of the inversion and Γ the temperature gradient of the geostrophic layer.

In this work, the trade-offs that arise between representing turbines using AD or AL methods are examined, with particular focus on whether and how the choice of model affects AGW development, and how the predicted impact of AGWs on the turbines depends on the actuator models employed. With the motivation of this work being primarily to identify if there are any fundamental differences in the dynamics relating to the actuator model gravity wave interactions, this work employs a uniform, non-turbulent inflow for the cases tested. Simplification of the inflow profile allows the elucidation of rotor-AGW interactions that can underpin future analysis of more complex flow cases by providing a baseline set of comparison cases. Additional atmospheric flow factors that could be studied could include gusting, sheared or non-uniform inflows, turbulent inflow and Coriolis forcing, all of which may impact results in different ways and to different extents.

2. Methodology

To compare the AL and AD turbine models, both were simulated under the same AGW conditions using the domain illustrated in Figure 2. The domain includes tuned Rayleigh damping regions in the geostrophic layer that are scaled with the predicted vertical AGW wavelength (λ_z) to minimise reflections [10, 11]. The domain width was 0.72 km with cyclic lateral boundaries, making the scenario equivalent to an infinitely wide turbine row with 3 diameter (D) spacing.

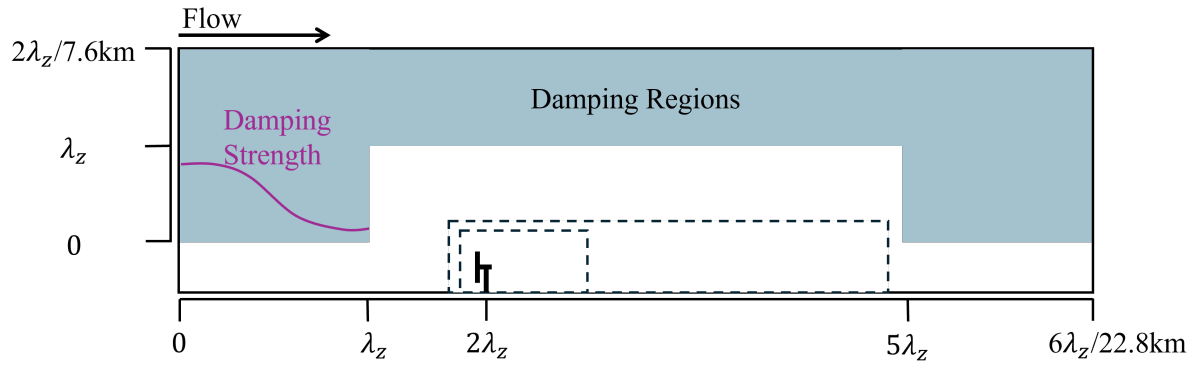

Figure 2: The simulation domain non-dimensionalised by the vertical AGW wavelength (λ_z), with shaded regions indicating damping and dashed boxes indicating mesh refinement regions.

The baseline mesh resolution was 20 m x 20 m horizontally and 10 m vertically up to twice the inversion layer height, beyond which the vertical cell dimension was gradually stretched to 300 m. The initial mesh resolution, set following the AGW literature, was refined around the turbine and wake region to effectively use the AL model [3, 5, 7, 9]. Two refinement regions were included, first to reduce the mesh resolution to a uniform 10 m cell size and second to 5 m (Δ_{cell}).

The length of each refinement region was tuned to best capture the far and near wake for all cases (45 D and 10 D respectively). These levels of refinement result in 24 cells or 48 cells across the rotor diameter, respectively, with both being on the upper limit of the resolution used in previous AGW simulations employing AD models [3, 6, 7, 9].

To isolate AGW effects from that of inflow turbulence, the investigation used a uniform 8 m/s inflow. The thermal inflow profile shown in Figure 1 was used with H=350 m, $\Delta\theta$=5 K , Γ=5 K/km and an inversion layer thickness of 100m so as to be representative of the North Sea [3].

2.1. Actuator Models

An in-house code, embedded in OpenFOAM, was used for the AL model, with its key parameters given in Table 1. The AL model used line average sampling, with further information on model parameters and their definitions extensively covered in the literature [12–15]. The exact values used herein were set based on initial testing and recommendations from the aforementioned literature.

Table 1: Key parameters of the AL model.

Sampling Distance	Collocation Points	Sampling Points	Smearing Kernel	Tip Loss Correction	Torque Controller
$1.1\cdot 3\cdot 2\Delta_{cell}$	100/D	16	Spherical Gaussian	Shen [16]	Yes

The AD model developed by Baungaard et al. [17] was also used to represent the turbine. This method applies a uniform thrust in a top-hat distribution over a cylindrical volume. In addition to the base model, a super Gaussian smearing kernel was added to avoid numerical instabilities generated in the force imposition region. The kernel (Ψ) smears the thrust in the axial and radial directions and takes the form of Equation 1

$$\Psi = \exp\left(-\left(\frac{x}{0.5\cdot t}\right)^{\alpha_r} - \left(\frac{r}{R}\right)^{\alpha_x}\right) \tag{1}$$

where t is the disk thickness, R is the disk radius, r and x are the radial and axial distances from the centre and α_r/α_x the smearing parameters. The smearing parameters, calibrated by Jané-Ippel et al. on experimental data, are adopted in this study [18]. The value of R was set to the radius of the turbine and T to be equivalent to a 4 cell thickness. For both the AD and AL methods the turbine characteristics were based on the IEA 15 MW turbine which has a diameter of 240 m [8].

2.2. Simulated Cases

The six cases simulated in this work are detailed in Table 2. The first three cases aimed to compare the AL and AD models directly by matching the AD thrust to that of the AL model. In case 3, the impact of mesh resolution was additionally explored by not including the inner mesh refinement box.

Table 2: Key parameters of the cases simulated

Case	Inflow	Mesh at Rotor	Model	C_T	Thrust (kN)
1	Uniform, 8 m/s	5 m	AL	Calculated	1180
2	Uniform, 8 m/s	5 m	AD	Set to AL	1180
3	Uniform, 8 m/s	10 m	AD	Set to AL	1180
4	Uniform, 8 m/s	5 m	AD	Set on specification [8]	1420
5	Uniform, 8 m/s	5 m	AD	10% above AL	1300
6	Uniform, 8 m/s	5 m	AD	10% below AL	1060

When using an AD model, it is not normally possible to calibrate the thrust based on a higher fidelity model. Instead, the thrust may be prescribed *a priori* from the turbine specifications for thrust coefficient and the imposed inflow velocity. This approach can be inaccurate because it cannot account for upstream flow deceleration caused by either the AGW enhanced farm blockage effect or another turbine's wake. A solution to this can be to adjust the thrust during the simulation through a local disk velocity and modified thrust coefficient, such as in the method developed by Calaf et al. [19, 20]. However, these methods often rely on 1D momentum theory to calibrate the thrust coefficient, which incorrectly assumes inviscid, steady flow. Furthermore, the disk velocity is commonly sampled at the same location as the force is applied. Together these factors again can lead to a mismatch between the true value and the predicted value for the thrust [20]. Therefore, cases 4 to 6 investigate the impact of varying the thrust coefficient (C_T) on the gravity waves that develop. The inflow velocity and 15 MW C_T specification were used to set the thrust in case 4 [8]. In cases 5 and 6 the thrust was varied to 10% above and below the AL value respectively.

All cases were run as Large Eddy Simulations using the OpenFOAM Buoyant Boussinesq PimpleFoam solver with a Smagorinsky model for the subgrid scale flow modelling. A second order backward scheme was used for the temporal discretisation and a second order central difference scheme for the convective term. Similar to previous studies, the simulations were run for 4000 s to ensure convergence and then the results were taken as the average over the following 2000 s [3, 9].

3. Results

3.1. Wake Recovery of Different Actuator Models

Figure 3 shows the wakes that develop behind the turbine when simulated with the AL (case 1) and AD (cases 2 and 3) models. The AGW impact on the turbine wakes is observed as an acceleration and deceleration of the flow speed in phase with the gravity wave troughs and peaks, respectively. Whilst wake recovery is observed in all cases, the recovery rate differs with the rotor model. The slower recovery of the AD wake in cases 2 and 3 when combined with the large spatial scale of gravity waves leads to a more pronounced effect of AGWs being observed than for the AL wake of case 1.

Although only one turbine row was modelled in the present study, the differences observed in simulated wake recovery would significantly impact the inferred performance of downstream turbines. In cases 2 and 3, a second turbine placed in line with a wave trough (e.g. dashed line in Figure 3) would still perform worse compared to the upstream turbine. However, in case 1 a second turbine could be expected to surpass the performance of the first turbine, as the mass flux through the rotor swept area is higher at this location than upstream of the local induction region of the first turbine (e.g. 5D). This predicted result in case 1, which is contrary to typical farm behaviour, arises from the AGW causing pockets of enhanced acceleration in the bypass flow above the wake and a deceleration upstream of the first turbine. Therefore, while differences in downstream turbine performance may arise simply from the ability of each model

to generate wake dynamics, the attenuation of AGW effects with streamwise distance adds an additional factor. This AGW attenuation means the extent to which an AGW may modify the flow for a downstream turbine to outperform an upstream one, is wake length and thus model dependent.

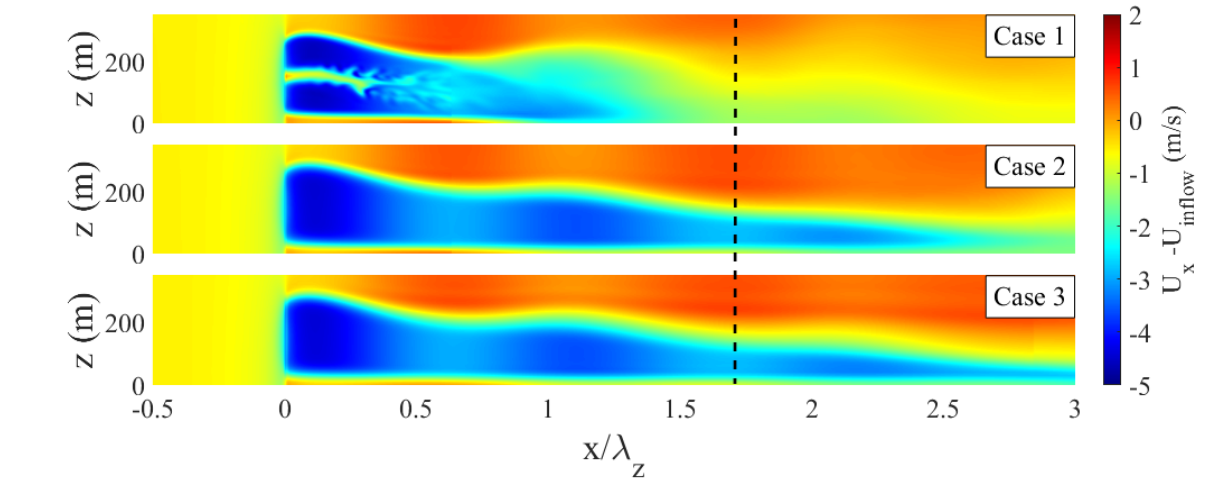

Figure 3: Time-averaged velocity deficit profiles for the AD and AL turbine models. The x-axis is defined relative to the turbine position and non-dimensionalised by the AGW wavelength (λ_z). The dashed line illustrates a position for a potential second turbine placement.

Figure 3 also highlights a difference in the simulated wake between the AD cases, with the higher mesh resolution in case 2 in closer agreement to the AL wake of case 1. This indicates that the wake resulting from the AD model is sensitive to mesh resolution, and that the most significant difference between the models could be the turbulence in the wake or the mechanisms governing wake breakdown. A comparison of the total Turbulent Kinetic Energy (TKE) in the wake supports this (Figure 4). Compared to cases 2 and 3, case 1 has a higher total TKE in the wake and a greater rate of increase in TKE over the wake. Case 2, which has the higher mesh resolution, is also closer to case 1 than the lower resolution case 3 is to case 1.

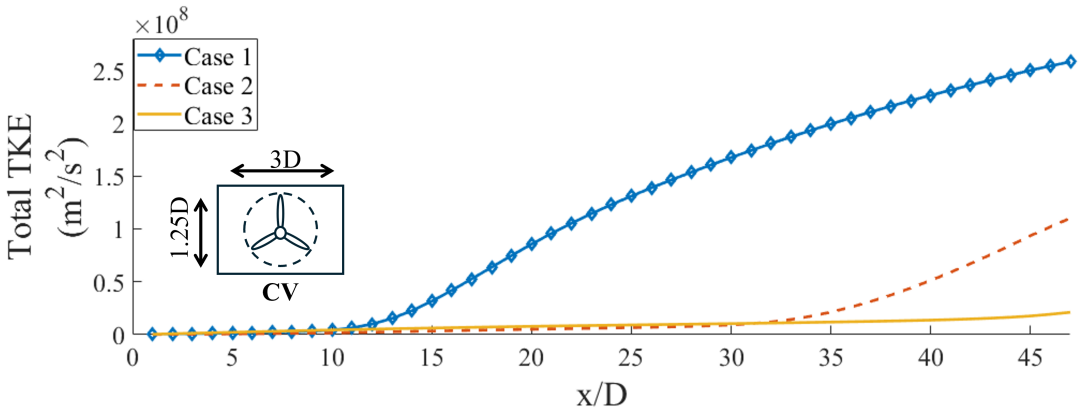

Figure 4: The total TKE in the turbine wake integrated over a Control Volume (CV) with increasing length in the streamwise direction (x).

The rate of TKE production (P_{TKE}) can be calculated using Equation 2,

$$P_{TKE} = \sum -\widetilde{u_i' u_j'} \frac{\partial \tilde{u}_i}{\partial x_j} \tag{2}$$

where u is the velocity, $\{\}'$ is used to denote the fluctuating component and $\tilde{\{\}}$ a time average.

This production term is shown for cases 1 to 3 in Figure 5, from which it is evident that in case 1 the TKE production both occurs earlier in the wake and is far stronger. This indicates that the cause of wake breakdown could be different for the AL model. The position and sudden increase in TKE production in the AL model suggests it is initiated when the turbine tip vortex structure collapses, a mechanism not captured in an AD model. By contrast, the AD results suggest the breakdown occurs as a result of an instability in the shear layer produced at the disk edges.

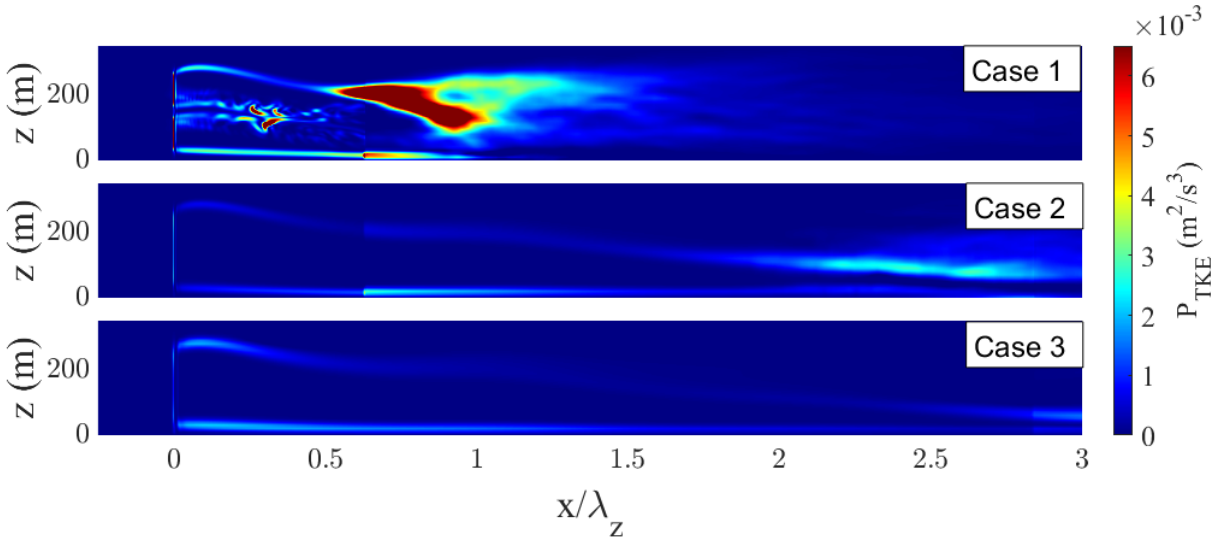

Figure 5: The rate of TKE production across the turbine wakes of cases 1 to 3. The x-axis is defined relative to the turbine position and non-dimensionalised by the AGW wavelength (λ_z).

3.2. Wave Fields of Different Actuator Models

The internal AGWs can be best visualised in the vertical velocity component of the flow field as shown in Figure 6 for cases 1 to 3.

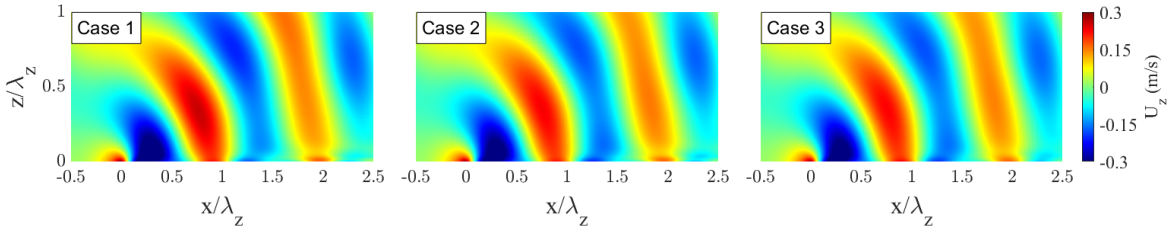

Figure 6: The vertical velocity field showing an internal gravity wave. The initial inversion layer top is the datum in the z direction and the turbine position is the datum in the x, both axis are non-dimensionalised by the AGW wavelength (λ_z).

The trapped waves in the inversion layer are shown through the perturbation to the background temperature profile in Figure 7, demonstrating the buoyancy-driven mechanism for the waves. From both Figures 6 and 7 it can be observed that the overall phase and shape of the wave field produced are independent of the turbine model used. This finding supports the use of low order models for predicting a wave field, potentially allowing the computational cost to be reduced when calibrating damping regions and domain sizes during AGW simulation setup.

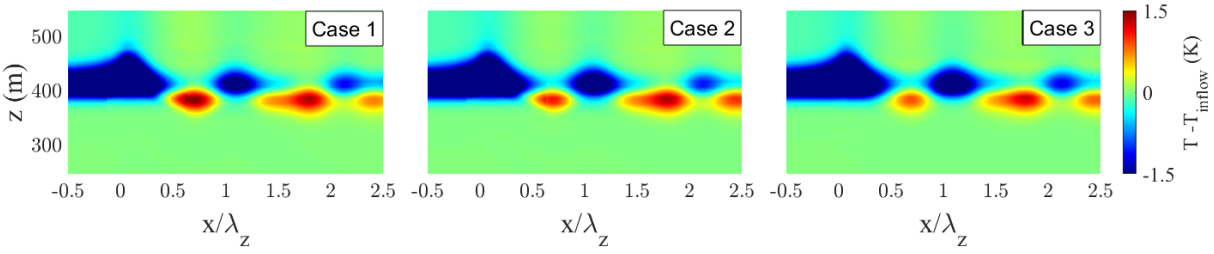

Figure 7: The perturbation to the temperature field, showing a trapped AGW. The x-axis is defined relative to the turbine position and non-dimensionalised by the AGW wavelength (λ_z).

Probing the vertical velocity field in the streamwise direction at an altitude of 1000 m and 2000 m in Figure 8 shows that the strength of the wave produced in the AL simulation was up to 12% higher than that of the AD at the first wave peak. This result is consistent with the stronger initial perturbations seen in the temperature field which shows there is a strong correlation between them. The exact reason behind these observed differences requires further investigation.

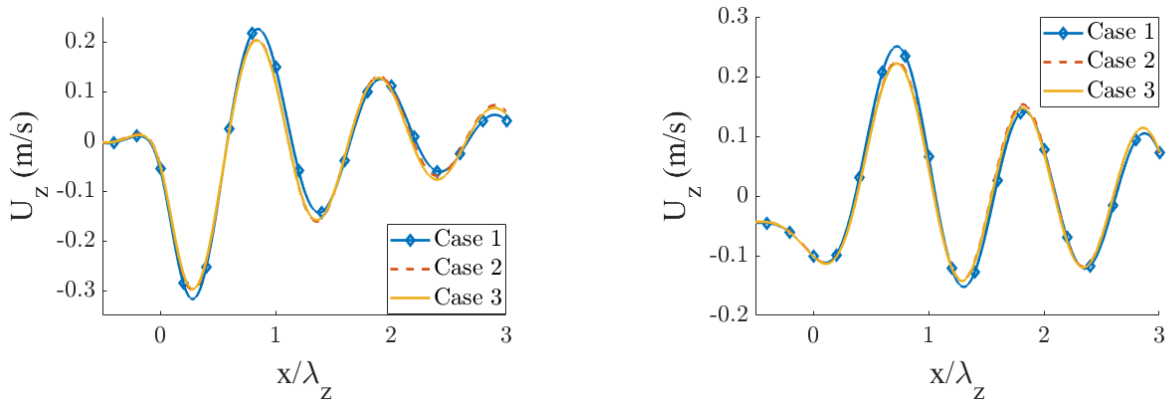

Figure 8: Vertical velocity profile in the streamwise direction at the centre of the domain taken at (a) 1000 m and (b) 2000 m. The x coordinates are taken in reference to the turbine position and non-dimensionalised by the AGW wavelength (λ_z).

3.3. Variation in Actuator Disk Thrust

For cases 4 to 6 the thrust of the actuator disk was varied with 4 being the highest and 6 the lowest. Changing the thrust resulted in the significant differences in AGW strength shown in Figure 9. This change in wave strength results from the higher disk thrust providing more

resistance to the flow, causing a greater vertical flow deflection around the disk and thus a stronger initial perturbation to generate the gravity wave. In addition to the change in strength of the wave, a small shift in wave phase is observed with thrust. This shift will have an effect on the exact positions of the gravity wave-induced acceleration and deceleration regions in the wake.

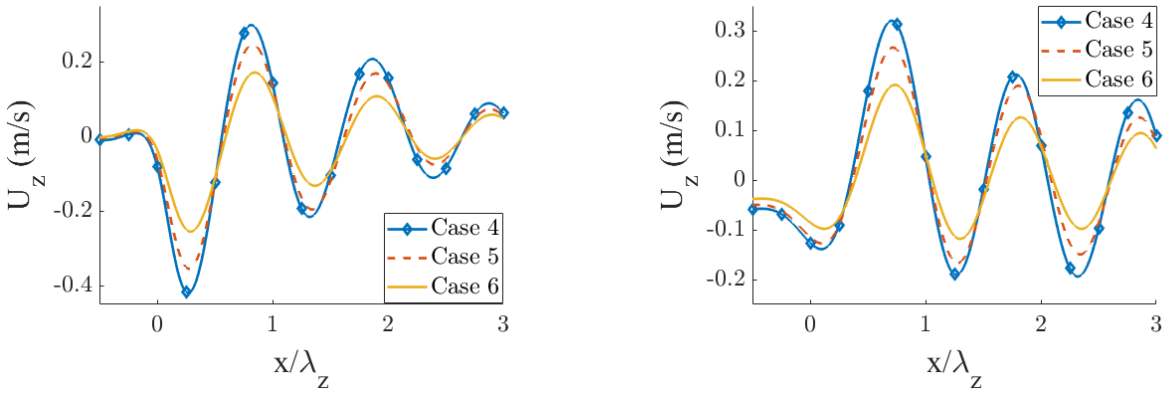

Figure 9: Vertical velocity profile in the streamwise direction at the centre of the domain taken at (a) 1000 m and (b) 2000 m. The x coordinates are taken in reference to the turbine position and non-dimensionalised by the AGW wavelength (λ_z).

One consequence of AGWs is an enhanced blockage effect, characterised by flow deceleration upstream of the turbines [4, 5], as can be seen in Figure 10. The magnitude of this deceleration is influenced by the wave strength. The streamwise velocity component at hub height 10 D upstream is reduced by 8.2, 7.3 and 6.0 % relative to the undisturbed inflow for cases 4, 5 and 6, respectively. Consequently, this wave enhanced blockage effect is shown to also be impacted by the prescribed thrust of the model.

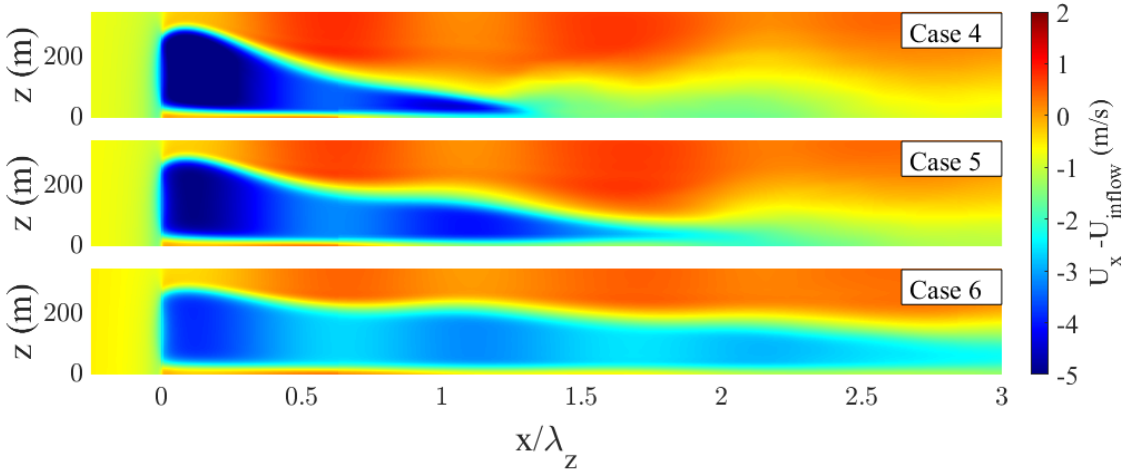

Figure 10: Time-averaged velocity deficit profiles for AD models with varying thrusts. The x-axis is defined relative to the turbine position and non-dimensionalised by the AGW wavelength (λ_z).

Varying disk thrust impacts the wakes that subsequently develop, as shown in Figure 10. Whilst normally the wake length would have been expected to have increased with turbine thrust, the presence of AGWs produces the opposite trend. A possible explanation for the faster wake recovery is the increased strength in the pockets of enhanced acceleration in the bypass flow above the wake in cases with higher turbine thrust. The stronger accelerations could be leading to increased shear stresses and thus higher transfer of momentum into the wake or act as a stronger perturbation to the wake, causing faster wake breakdown. The pockets of acceleration are caused by the inversion layer vertically confining the flow and as such, at a wave trough the flow below the inversion accelerates to satisfy mass conservation [21]. Therefore, with greater displacement of the inversion layer associated with a stronger wave, the bypass accelerations are also a function of wave strength and thus the thrust.

Along the streamwise direction, changes in wake height associated with AGW peaks and troughs are also more extreme in cases 4 and 5 when compared to case 6, which has the lower thrust and wave strength. The difference between the peaks and troughs in the wake velocity for case 5 are also greater than those of case 6 because of the wave being stronger. This demonstrates that the accuracy of predicting the thrust for the AD model will have a significant impact on both the wake and AGW wave field, which importantly are also coupled.

Finally, these results suggest that for farm scale simulations different predictions of both individual-turbine and overall farm performance may result from a change in turbine thrust modifying the AGW field and thereby influencing the predicted wake interactions and the wave-enhanced farm-blockage effect. Consequently, the farm performance under AGWs may not just be a function of the atmospheric conditions but also the way in which thrust is distributed throughout it as a result of the farm operation or design.

4. Conclusion

This study has shown that the choice of turbine model and its parameters can have an impact on both the AGW produced and its effect on the wake of the wind turbines. The difference in the simulated wake between the actuator line and actuator disk models was driven by the TKE generated in the wake, which varied significantly between cases. The contrast in these results implies that the current AD model does not capture the full complexity of the AL wake dynamics, which results in the slower wake break down when compared to the AL model. The difference in wake recovery altered the streamwise extent of the AGW and wake interactions which could have implications for the performance of a downstream turbine. This finding indicates that the actuator model choice for turbine representation may impact the predicted performance of a farm under AGW conditions through a difference in the predicted wake interactions. Consequently, this work both supports and motivates further investigation with farm simulations incorporating additional atmospheric physics, such as turbulent inflow conditions, to evaluate the full extent of these differences.

The wake produced by the AD model was found to be sensitive to its two key setup parameters, the thrust coefficient and mesh resolution at the rotor. Previous AGW studies have used less than half the number of cells across the rotor of the coarsest case in this study and anisotropic meshes at the rotor plane [3, 6, 7, 9]. The discrepancy in results shown here between isotropic meshes which had higher mesh refinement indicates caution should be used when using lower resolution simulations for planning farms where minimising wake interaction is being optimised. Nevertheless, the independence of the simulated AGW field shape and phase from the actuator model and mesh resolution employed, supports the use of coarser models when considering AGWs at the farm and global scale. Whilst differences in wave strength were observed, through the evaluation of the perturbed vertical velocity profile of the geostrophic layer, these were small compared to the difference that was seen by a change in rotor thrust.

The magnitude of turbine thrust was shown to have the biggest impact on the wakes and

AGW. Moreover, as a result of the wake and wave dynamics being interconnected, the variation in results for the turbines with different thrusts was amplified. For AGW simulations, this means that even if more complex and higher fidelity actuator models are used, the validity of the results both on the turbine and farm scale relies on the fundamental ability to accurately specify the thrust. Consequently, the effect on a farm scale AGW simulation of changes in turbine thrust, through the choice of turbine control and the inevitable variations in wind speed, is an area worthy of further investigation.

Acknowledgments
This work used the ARCHER2 Supercomputing Service through the Wake Aerodynamics of Offshore Wind Turbines (WAFT) project funded by the EPSRC. The authors acknowledge funding from CRV's UKRI Future Leaders Fellowship (MR/V02504X/1) and through TR's Margaret Thatcher Scholarship.

References

[1] Porté-Agel F, Bastankhah M and Shamsoddin S 2020 *Boundary-layer meteorology* **174** 1–59
[2] Wallace J M and Hobbs P V 2006 *Atmospheric Science* (Academic Press) pp 63–111 2nd ed
[3] Lanzilao L and Meyers J 2024 *J. of Fluid Mechanics* **979** A54
[4] Wu K L and Porté-Agel F 2017 *Energies* **10** 2164
[5] Stipa S, Ajay A, Allaerts D and Brinkerhoff J 2024 *Wind Energy Science* **9** 297–320
[6] Lanzilao L and Meyers J 2022 *J. Phys.: Conf. Series* **2265** 022043
[7] Maas O 2023 *Frontiers in Mechanical Engineering* **9** 1108180
[8] Gaertner E *et al.* 2020 Tech. rep. National Renewable Energy Lab. (NREL), Golden, CO (United States)
[9] Allaerts D and Meyers J 2017 *Journal of Fluid Mechanics* **814** 95–130
[10] Khan M A, Allaerts D, Watson S J and Churchfield M J 2025 *Wind Energy Science* **10** 1167–1185
[11] Lanzilao L and Meyers J 2023 *Boundary-layer meteorology* **186** 567–593
[12] Sorensen J N and Shen W Z 2002 *J. of Fluids Eng* **124** 393–399
[13] Zormpa M, Zilic de Arcos F, Chen X, Vogel C R and Willden R H J 2025 *Wind Energy* **28** e2965
[14] Troldborg N, Sorensen J N and Mikkelsen R 2010 *Wind Energy* **13** 86–99
[15] Liu L, Franceschini L, Oliveira D F, Galeazzo F C, Carmo B S and Stevens R J A M 2022 *Wind Energy* **25** 1046–1059
[16] Shen W Z, Mikkelsen R, Sørensen J N and Bak C 2005 *Wind Energy* **8** 457–475
[17] Baungaard M, Nishino T and van der Laan M P 2025 *Wind Energ. Sci. Discuss.* [Preprint]
[18] Jané-Ippel C, Bempedelis N, Palacios R and Laizet S 2024 *Wind Energy* **27** 1412–1426
[19] Calaf M, Meneveau C and Meyers J 2010 *Phys. of Fluids* **22** 015110
[20] van der Laan M P, Sørensen N N, Réthoré P E, Mann J, Kelly M C and Troldborg N 2015 *Wind Energy* **18** 2223–2240
[21] Stipa S, Ahmed Khan M, Allaerts D and Brinkerhoff J 2024 *Wind Energy Science* **9** 1647–1668